J Appl Electrochem (2010) 40:709–718
DOI 10.1007/s10800-009-0048-3

ORIGINAL PAPER

# Theoretical and experimental study of electrochemical reactors with three-dimensional bipolar electrodes

**O. González Pérez · J. M. Bisang**

Received: 17 August 2009 / Accepted: 1 December 2009 / Published online: 19 December 2009
© Springer Science+Business Media B.V. 2009

**Abstract** A mathematical model to represent three-dimensional bipolar electrodes is proposed taken into account the leakage current. The model is analytically solved when the electrochemical reaction has a mass-transfer control at low overpotentials, which represents a limiting case of the general mathematical treatment. For this simplified situation, expressions are deduced to evaluate the current and potential distribution and to calculate the leakage current. The effect on the leakage current of kinetic, electrochemical and geometric variables, which are lumped into one dimensionless number, is discussed. The influence of the leakage current on the optimal bed depth under limiting current conditions is also analyzed. Likewise, experimental data, using the deposition–dissolution of copper as test reaction, are compared with the theoretical prediction of the general treatment achieving a good agreement between both.

**Keywords** Bipolar electrodes · Current distribution · Electrochemical reactors · Leakage current · Three-dimensional electrodes

## List of symbols

### Variables

| | |
|---|---|
| $A_s$ | Surface area per unit electrode volume ($m^{-1}$) |
| $C$ | Concentration (mol $m^{-3}$, mol $dm^{-3}$ or ppm) |
| $d$ | Wire diameter (m) |
| $D$ | Diffusion coefficient ($m^2$ $s^{-1}$) |
| $E_0$ | Reversible electrode potential (V) |
| $E_0^0$ | Reversible electrode potential under standard conditions (V) |
| F | Faraday constant (C $mol^{-1}$) |
| $i$ | Current density (A $m^{-2}$) |
| $I$ | Total current (A) |
| $I^*$ | Leakage current (A) |
| $j$ | Reaction rate (A $m^{-2}$) |
| $j_d$ | j-factor for mass transfer $= k_m/(u/\varepsilon)$ $Sc^{2/3}$ |
| $j_0$ | Exchange current density (A $m^{-2}$) |
| $j_L$ | Limiting current density (A $m^{-2}$) |
| $k_m$ | Mass-transfer coefficient (m $s^{-1}$) |
| $L$ | Thickness of the bipolar electrode (m) |
| $L_c$ | Thickness of the cathodic part at the bipolar electrode (m) |
| $M$ | Atomic weight (kg $mol^{-1}$) |
| RT/F | Constant (0.0261 V at 30 °C) (V) |
| Re | Reynolds number $= ud/(\varepsilon v)$ |
| $R_p$ | Polarization resistance (Ω) |
| $R_s$ | Electrolyte resistance (Ω) |
| $S$ | Membrane area ($m^2$) |
| Sc | Schmidt number $= v/D$ |
| $t$ | Time of the experiment (s or min) |
| $u$ | Superficial electrolyte flow velocity (m $s^{-1}$) |
| Wa | Wagner number |
| $x$ | Axial coordinate (m) |
| $y$ | Axial coordinate (m) |
| $z$ | Axial coordinate (m) |

### Greek characters

| | |
|---|---|
| $\beta$ | Charge-transfer coefficient |
| $\gamma$ | Activity coefficient |
| $\delta$ | Density (kg $m^{-3}$) |
| $\Delta r$ | Change in the wire radius (m) |

O. González Pérez · J. M. Bisang (✉)
Programa de Electroquímica Aplicada e Ingeniería Electroquímica (PRELINE), Facultad de Ingeniería Química, Universidad Nacional del Litoral, Santiago del Estero 2829, 3000AOM Santa Fe, Argentina
e-mail: jbisang@fiq.unl.edu.ar

$\varepsilon$ Porosity
$\eta$ Overpotential (V)
$v$ Kinematic viscosity ($m^2\ s^{-1}$)
$v_e$ Charge number of the electrode reaction
$\rho$ Effective resistivity ($\Omega$ m)
$\rho^0$ Electrolyte resistivity ($\Omega$ m)
$\phi$ Potential (V)
$\psi$ By-passed fraction of the total current defined by Eq. 30
$\Omega$ Parameter given by Eq. 20

**Subscripts**

exp Experimental
m Metal phase
s Solution phase
th Theoretical

## 1 Introduction

Increasingly stringent legislation for effluents calls for reliable and cost-efficient processes for the purification of waste water. Electrochemistry can offer alternatives which compete favourably with more common technologies. Likewise, some electrochemical production processes take place under mass transport control at low rates to be carried out in conventional electrochemical reactors. Thus, three-dimensional electrodes are used to increase the production per unit of reactor volume. These electrodes are frequently proposed with a monopolar arrangement, where the electrodes have a single polarity, either anodes or cathodes. In spite of the good performance of these devices, an external electrical connection at each electrode of the reactor is required, which can be troublesome for some three-dimensional structures. In order to circumvent this difficulty, a bipolar connection is attractive. Electrochemical reactors with bipolar parallel plate electrodes are profusely used in the industrial practice, and the state of the art is properly shown by Pletcher and Walsh [1]. However, the modelling of electrochemical reactors with three-dimensional bipolar electrodes is scarcely treated in the literature, and some contributions are summarized in [2]. Also, Alkire [3] presented a pioneering work related to the theoretical study of porous bipolar electrodes, which are considered to be the overlapping of two continua: the solution phase and the metal phase. The overpotential and concentration distributions are obtained by numerical solution of the differential equations assuming a single reaction with a combined diffusion and charge-transfer kinetic control. The influence of the system parameters on the reaction rate distribution is discussed. However, the effect of the leakage current has been disregarded. Fleischmann and Ibrisagić [4] have extended the model to bipolar trickle bed reactors. Goodridge et al. [5, 6] and Goodridge [7] studied the behaviour of conductive particles set in an electrical field. In [5], the particles are mechanically isolated between them, whereas in [6, 7] the separation of the particles is achieved by fluidization. These contributions give more attention to the specific energy consumption of the reactors and the theoretical values are compared with experimental ones obtained using the production of hypochlorite, hypobromite, epoxidation of styrene and synthesis of dimethyl sebacate as test reactions. Kusakabe et al. [8, 9] measured separately the faradaic current in the particulate phase, the leakage or by-pass current in the electrolyte phase and the short-circuiting current in regularly and randomly bipolar packed-bed electrodes. An inert bed of non-conducting pellets was used to measure the leakage current. Miyazaki et al. [10] presented a method to simulate the potential and current distribution in an electrochemical reactor with spherical conductive particles. The solution was simulated by a conductive paper and the kinetics at the electrode surface by an electric circuit. It was concluded that the simulator was appropriate to represent the reactors. Sasaki and Ishikawa [11] measured the faradaic current in a bipolar disk reactor with many holes using a split electrode, the results are interpreted with a network model, and it was concluded that the by-pass resistance increases with the applied current. Moreover, Cheng et al. [12] reported the modelling of potentials, concentrations and current densities for flow through porous electrodes with monopolar or bipolar electric connections. For the removal of Pb(II) ions, the monopolar system showed the best performance due to the leakage currents in the bipolar arrangement. The bipolar three-dimensional electrodes are generally used with a stationary configuration of electrodes. However, Sasaki and Ishikawa [13] studied the copper deposition from dilute solutions with a rotating bipolar cell made up of disc electrodes with fins attached to the anode to promote turbulence and scrape the deposited metal. Furthermore, to vary the electrode potential by mechanically moving a cylindrical electrode through different potential regions, Nadebaum et al. [14, 15] have employed a rotating bipolar electrode. Several authors have studied the production of substances using bipolar three-dimensional electrodes. Thus, Fleischmann et al. [16] reported the reduction of 2-nitropropane to isopropylhydroxylamine and isopropylamine in an undivided, flooded, bipolar reactor. Bakir Ogutveren et al. [17] have investigated the production of Co(III) acetate using a bipolar trickle tower of graphite Raschig rings with the purpose of the regeneration of catalysts. With the same aim, Güvenc et al. [18] reported that a bipolar packed-bed reactor is suitable for the oxidation of Mn(II) acetate. Boussoulengas et al. [19], Ellis and Jansson [20] and Franke et al. [21] investigated the production of propylene oxide using a bipolar trickle tower. Kim et al. [22] reported the reaction

kinetics, current efficiency and energy consumption for the electrochemical methoxylation of *p-tert*-butyltoluene with a bipolar packed-bed electrode cell. The electro-synthesis of alkaline peroxide in a bipolar reactor was studied by Gupta and Oloman [23]. Likewise, due to their simple electrical arrangement, bipolar electrochemical reactors with three-dimensional electrodes have been proposed for effluent treatment. Thus, Ehdaie et al. [24] reported the scavenging of metal ions with a bipolar trickle tower, and Cox et al. [25] analyzed a similar device for the treatment of effluents from adipic acid plants. The electrochemical reduction of copper ions in bipolar systems was studied in [26]. Grau and Bisang [27] recently reported the behaviour of a bipolar electrochemical reactor consisting of a rotating cylindrical electrode of woven-wire meshes for copper or cadmium deposition from dilute solutions.

Taken into account that bipolar electrochemical reactors with three-dimensional electrodes represent promising devices for industrial practice, the aim of the present study is to contribute to the modelling of these reactors, considering the effect of the leakage currents on the current distribution, and to compare the theoretical data with experimental results to determine the predictive suitability of the mathematical model.

## 2 Mathematical modelling

### 2.1 General treatment

Figure 1 schematically shows a bipolar three-dimensional electrode placed between two terminal electrodes, where a diagram of the variation of the current in the solution and metal phases is also given. In the following theoretical analysis, some simplifying assumptions are made:

(i) The specific surface area and the porosity of the three-dimensional structure are uniform.
(ii) The variation of overpotential occurs along a single spatial dimension, $x$ coordinate.
(iii) Only one reversible electrochemical reaction, under combined diffusion and charge-transfer kinetic control, takes place. Thus, the concentration variation is not taken into account. Although, this kinetic expression restricts the application of the model its essential features are maintained, and the calculation procedure is illustrated.
(iv) Operation proceeds in the steady-state without structural changes in the electrode. Thus, properties of the electrodes remain constant with time. For deposition–dissolution of metals the specific surface area and the porosity are modified during the experiment. In this case, the present model represents a first approach for the reactor calculation.

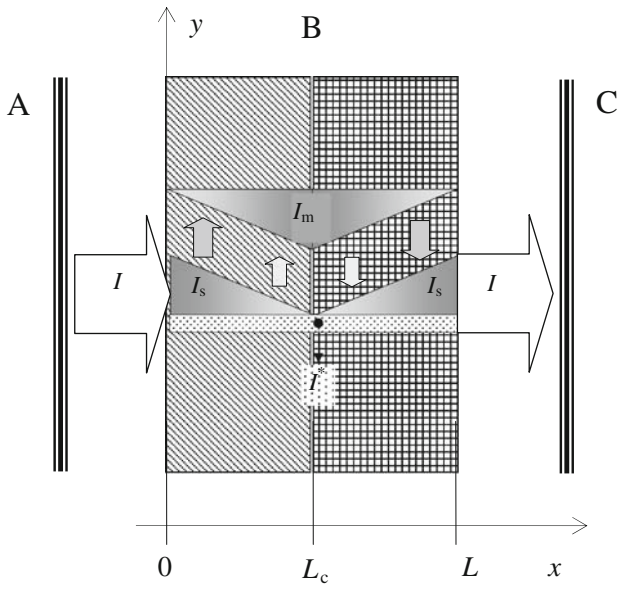


**Fig. 1** Diagram of an electrochemical stack with one bipolar three-dimensional electrode. *A*—terminal anode, *B*—bipolar electrode and *C*—terminal cathode. Inset: schematic representation of the current variations in the metal and solution phases inside the bipolar electrode

(v) The migration of the reactive species is disregarded due to the presence of a supporting electrolyte.
(vi) The effective resistivity of the metal phase is negligible in comparison with that of the solution phase.

The current balance in the solution phase yields

$$\frac{\mathrm{d}i_s(x)}{\mathrm{d}x} = A_s j(x). \tag{1}$$

The Ohm's law for the solution phase is

$$\frac{\mathrm{d}\phi_s(x)}{\mathrm{d}x} = -\rho_s i_s(x). \tag{2}$$

Assuming the metal phase as isopotential the overpotential is given by

$$\eta(x) = \phi_m - \phi_s(x) - E_0. \tag{3}$$

Combining Eqs. 1–3 results in the following differential equation

$$\frac{\mathrm{d}^2\eta(x)}{\mathrm{d}x^2} = \rho_s A_s j(x), \tag{4}$$

with the boundary conditions

$$\text{at } x = 0 \text{ is } \left.\frac{\mathrm{d}\eta}{\mathrm{d}x}\right|_{x=0} = \rho_s \frac{I}{S} \tag{5}$$

$$\text{at } x = L \text{ is } \left.\frac{\mathrm{d}\eta}{\mathrm{d}x}\right|_{x=L} = \rho_s \frac{I}{S}. \tag{6}$$

Integrating Eq. 1, it is obtained

$$i_s(x) - \frac{I^*}{S} = -A_s \int_x^{L_c} j(x)\ \mathrm{d}x, \tag{7}$$

where $I^*$ is the leakage current, which by-passes the bipolar electrode. Evaluating Eq. 7 at $x = 0$, the current at the cathodic side of the bipolar electrode results in

$$I_{\text{cathodic side}} = \frac{I}{S} - \frac{I^*}{S} = -A_s \int_0^{L_c} j(x)\ \mathrm{d}x. \tag{8}$$

Analogously, the current at the anodic side is

$$I_{\text{anodic side}} = \frac{I}{S} - \frac{I^*}{S} = A_s \int_{L_c}^{L} j(x)\ \mathrm{d}x. \tag{9}$$

Combining Eq. 7 with Eqs. 2 and 3 and rearranging yields

$$\left.\frac{\mathrm{d}\eta(x)}{\mathrm{d}x}\right|_x = \frac{I^*\rho_s}{S} - \rho_s A_s \int_x^{L_c} j(x)\ \mathrm{d}x. \tag{10}$$

The evaluation of Eq. 10 at $x = L_c$, when the overpotential is zero, allows the calculation of the leakage current according to

$$I^* = \frac{S}{\rho_s}\left.\frac{\mathrm{d}\eta}{\mathrm{d}x}\right|_{x=L_c}. \tag{11}$$

Adopting for the kinetics a combined diffusion and charge-transfer expression according to

$$j(x) = \frac{\exp\left[\frac{\nu_e F}{RT}\eta(x)\right] - 1}{\exp\left[\frac{\beta F}{RT}\eta(x)\right]/j_0 - 1/j_L}. \tag{12}$$

Thus, $j$ is negative for the cathodic part and positive for the anodic one. Being

$$j_L = -\nu_e F k_m C. \tag{13}$$

Several equations are proposed in the literature to calculate the mass-transfer coefficient in three-dimensional electrodes of woven-wire meshes, which were summarized by Cœuret and Storck [28]. However, in these calculations the correlation proposed by Storck et al. [29] was used because it corresponds to the case of current and electrolyte flows at right angles, according to:

$$j_d = 0.4\mathrm{Re}^{-0.507}. \tag{14}$$

However, for deposition–dissolution of metals at the bipolar electrode, the so calculated mass-transfer coefficient represents a conservative value because the properties of the electrode are altered during the experiment in a non-predicted manner.

Further equations to solve the mathematical treatment are the Bruggeman relationship to calculate the effective electrolyte resistivity:

$$\rho_s = \rho^0 \varepsilon^{-3/2}, \tag{15}$$

and the reversible electrode potential is given by the Nernst equation

$$E_0 = E_0^0 + \frac{RT}{\nu_e F}\ln C\gamma. \tag{16}$$

The activity coefficient of the cupric ions was assumed equal to the mean ionic activity coefficient of the cupric sulphate, which was estimated according to the method of Kusik and Meissner [30].

The simultaneous and iterative solution of Eqs. 4, 8 and 11–16 allows the calculation of the potential and current distribution, total current and leakage current for a bipolar three-dimensional electrode. These calculations were performed using the finite difference method. The calculation procedure is shown in more detail in Fig. 2. Table 1

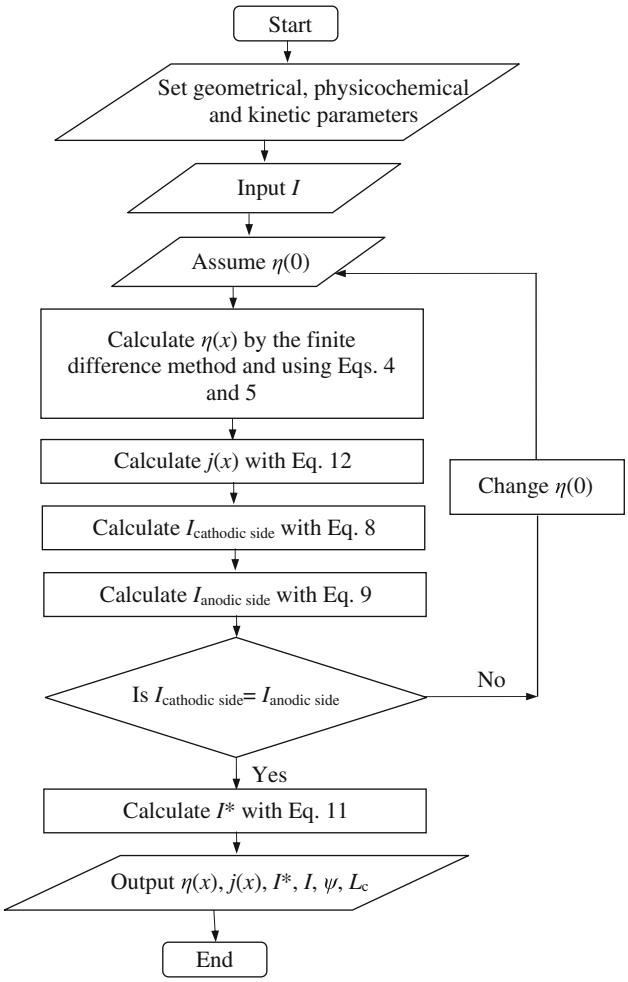


**Fig. 2** Flow chart illustrating the calculation procedure

**Table 1** Physicochemical properties and kinetic parameters used in modelling

| | |
|---|---|
| $\rho^{\circ}$ ($\Omega$ m) | $9.5 \times 10^{-2}$ |
| $v$ ($m^2\ s^{-1}$) | $1.11 \times 10^{-6}$ |
| $D$ ($m^2\ s^{-1}$) | $[7.35–5.3C^{0.5}$ (mol $dm^{-3}$)] $\times 10^{-10}$ |
| $\delta_{Cu}$ (kg $m^{-3}$) | $8.88 \times 10^{3}$ |
| $E_0^0$ (V vs. SCE) | 0.1 |
| $\gamma_{Cu}^{+2}$ | 0.0414 |
| $j_0$ (A $m^{-2}$) | $1.13 \times 10^{-2}\ C^{0.82}$ (ppm) |
| $\beta$ | 0.36 |
| $v_e$ | 2 |

summarizes the physicochemical properties and kinetic parameters used in the calculations.

## 2.2 Reaction controlled by mass-transfer at low overpotentials

As the rigorous calculations are cumbersome, in the following deduction, the above mathematical treatment will be solved considering for the kinetics a mass-transfer controlled expression according to

$$j(x) = j_L\left\{1 - \exp\left[\frac{v_e F}{RT}\eta(x)\right]\right\}. \tag{17}$$

At low overpotentials Eq. 17 is simplified to

$$j(x) = |j_L|\frac{v_e F}{RT}\eta(x). \tag{18}$$

Introducing Eq. 18 into Eq. 4 results in

$$\frac{d^2\eta(x)}{dx^2} = \Omega^2\eta(x) \tag{19}$$

being

$$\Omega^2 = \rho_s A_s |j_L|\frac{v_e F}{RT}. \tag{20}$$

Solving Eq. 19 with the boundary conditions given by Eqs. 5 and 6 results for the overpotential distribution inside the bipolar electrode

$$\eta(x) = \eta(0)\frac{\sinh\left[\Omega\left(\frac{L}{2} - x\right)\right]}{\sinh\left(\frac{\Omega L}{2}\right)}. \tag{21}$$

Evaluating Eq. 21 at $x = L/2$ is $\eta(L/2) = 0$. Therefore, for this kinetic control $L_c = L/2$. Combining Eqs. 18 and 21, the current distribution is given by

$$j(x) = |j_L|\frac{v_e F}{RT}\eta(0)\frac{\sinh\left[\Omega\left(\frac{L}{2} - x\right)\right]}{\sinh\left(\frac{\Omega L}{2}\right)}. \tag{22}$$

Introducing Eq. 22 into Eq. 8, solving and rearranging results in

$$I - I^* = \frac{\Omega S|\eta(0)|}{\rho_s}\frac{\cosh\left(\frac{\Omega L}{2}\right) - 1}{\sinh\left(\frac{\Omega L}{2}\right)}. \tag{23}$$

Likewise, introducing the first derivative of Eq. 21, evaluated at $x = L/2$, into Eq. 11 and rearranging yields

$$I^* = \frac{\Omega S|\eta(0)|}{\rho_s \sinh\left(\frac{\Omega L}{2}\right)}. \tag{24}$$

For small values of the argument is

$$\sinh\left(\frac{\Omega L}{2}\right) \cong \frac{\Omega L}{2}. \tag{25}$$

Introducing Eq. 25 in Eq. 24 results in

$$I^* = \frac{2S|\eta(0)|}{\rho_s L} = \frac{S}{\rho_s L}[\phi_s(0) - \phi_s(L)] \tag{26}$$

and combining Eqs. 21 and 25 is

$$\eta(x) = \eta(0)\left(1 - \frac{2x}{L}\right). \tag{27}$$

Equation 26 gives the leakage current for a three-dimensional bipolar electrode when the overpotential distribution in the bed is linear, Eq. 27, which coincides with the expected current through an inert bed. Therefore, combining Eqs. 24 and 26 leads to

$$\frac{I^*|_{\text{bipolar electrode}}}{I^*|_{\text{inert bed}}} = \frac{\frac{\Omega L}{2}}{\sinh\left(\frac{\Omega L}{2}\right)}. \tag{28}$$

Equation 28 shows that the leakage current in a bipolar electrode is always smaller than the current through an inert bed with the same geometric characteristics. Both currents only coincide for small values of $\frac{\Omega L}{2}$; for which, according to Eq. 27, a linear overpotential distribution is obtained. Therefore, the leakage current in a bipolar three-dimensional electrode cannot be obtained from a separate experiment with an inert bed of identical geometric dimensions because the faradaic current and the leakage current are coupled in an active electrode. Thus, the leakage current modifies the potential distribution inside the electrode and alters the faradaic current, but at the same time, the faradaic current changes the potential gradient in the solution phase and diminishes the leakage current. Experimental measurements performed with an inert bed allow only the estimate of the maximum value of the leakage current for the system.

Introducing Eq. 24 into Eq. 23 results for the total current

$$I = \frac{\Omega S|\eta(0)|}{\rho_s}\frac{\cosh\left(\frac{\Omega L}{2}\right)}{\sinh\left(\frac{\Omega L}{2}\right)}. \tag{29}$$

The by-passed fraction of the total current is defined by Burnet and Danly [31] as

$$\psi = \frac{I^*}{I}. \tag{30}$$

Combining Eqs. 24 and 29 yields

$$\psi = \frac{1}{\cosh\left(\frac{\Omega L}{2}\right)}. \tag{31}$$

The by-passed fraction of the total current, $\psi$, is a function of the dimensionless number $\Omega L$, which depends on the geometry of the electrode, the resistivity of the electrolyte and the kinetic parameters of the reaction. The Wagner number [32] is defined as the ratio of polarization and electrolyte resistance:

$$\mathrm{Wa} = \frac{R_\mathrm{p}}{R_\mathrm{s}} \tag{32}$$

being

$$R_\mathrm{s} = \frac{\rho_\mathrm{s} L}{S}. \tag{33}$$

And, taking the first derivative of Eq. 18 is

$$R_\mathrm{p} = \frac{\mathrm{d}\eta}{\mathrm{d}I} = \frac{\mathrm{R}T}{v_\mathrm{e}\mathrm{F}|j_\mathrm{L}|A_\mathrm{s}SL}. \tag{34}$$

Introducing Eqs. 33 and 34 in Eq. 32 yields

$$\mathrm{Wa} = \frac{\mathrm{R}T}{\rho_\mathrm{s} v_\mathrm{e}\mathrm{F}|j_\mathrm{L}|A_\mathrm{s}L^2}. \tag{35}$$

Comparing Eqs. 20 and 34 results

$$\sqrt{\mathrm{Wa}} = \frac{1}{\Omega L}. \tag{36}$$

In this way, all parameters, which have an influence on the current distribution and on the by-passed fraction of the total current, combine in a single dimensionless variable similar to that used in current distribution problems for other electrochemical systems.

According to Eqs. 31 and 36, a decrease in the Wagner number diminishes the fraction of the leakage current. Therefore, $\psi$ markedly decreases when the effective electrolyte resistivity increases. Thus, for a bipolar three-dimensional electrode it may be convenient to allow the generation of gases, as side reactions inside the electrode, so as to reduce the by-passed fraction of current due to the increase in the effective resistivity. A withdrawal of this proposal is the decrease of the current efficiency. Likewise, a material with a higher specific surface area must be adopted to diminish the by-passed fraction of current. The processing of very dilute solutions, characterized by a low limiting current density will produce high $\psi$. In order to counteract this deleterious aspect, it is necessary to choose intricate materials to make the three-dimensional electrode to increase the mass-transfer coefficient due to its turbulence promoting action. Similarly, high bed thickness improves the performance of the electrode. Taken into account Eq. 31, for a reaction under mass-transfer control at low overpotentials, when $\Omega L/2$ is higher than 3, the leakage current represents about 10% of the total current.

### 2.3 Reaction controlled by mass-transfer at limiting current conditions in the cathodic side: optimum bed depth

When the cathodic overpotential at $x = 0$ becomes quite negative, most of the cathodic side is working under limiting current conditions. Thus, for the cathodic side Eq. 17 is

$$j(x) = j_\mathrm{L} \tag{37}$$

introducing Eq. 37 in Eq. 4, and solving with the following boundary conditions at $x = 0$

$$\eta = \eta(0) \quad \text{and} \quad \left.\frac{\mathrm{d}\eta}{\mathrm{d}x}\right|_{x=0} = \rho_\mathrm{s}\frac{I}{S} \tag{38}$$

it results in

$$\eta(x) = \eta(0) + \rho_\mathrm{s}\frac{I}{S}x - \rho_\mathrm{s}A_\mathrm{s}|j_\mathrm{L}|\frac{x^2}{2}. \tag{39}$$

Introducing Eq. 37 in Eq. 8 and solving

$$\frac{I}{S} = \frac{I^*}{S} + A_\mathrm{s}|j_\mathrm{L}|L_\mathrm{c}. \tag{40}$$

Combining Eqs. 39 and 40 and evaluating at $x = L_\mathrm{c}$

$$\eta(L_\mathrm{c}) = \eta(0) + \rho_\mathrm{s}\left(\frac{I^*}{S} + A_\mathrm{s}|j_\mathrm{L}|L_\mathrm{c}\right)L_\mathrm{c} - \rho_\mathrm{s}A_\mathrm{s}|j_\mathrm{L}|\frac{L_\mathrm{c}^2}{2}. \tag{41}$$

Rearranging Eq. 41, yields for the cathodic bed thickness

$$L_\mathrm{c} = -\frac{I^*}{SA_\mathrm{s}|j_\mathrm{L}|} + \sqrt{\left(\frac{I^*}{SA_\mathrm{s}|j_\mathrm{L}|}\right)^2 + \frac{2[\eta(L_\mathrm{c}) - \eta(0)]}{\rho_\mathrm{s}A_\mathrm{s}|j_\mathrm{L}|}}. \tag{42}$$

When $I^* = 0$, Eq. 42 is simplified to

$$L_\mathrm{c} = \sqrt{\frac{2[\eta(L_\mathrm{c}) - \eta(0)]}{\rho_\mathrm{s}A_\mathrm{s}|j_\mathrm{L}|}}. \tag{43}$$

Thus, the optimal bed thickness for a monopolar three-dimensional electrode, according to Kreysa [33], is recovered. Comparing Eqs. 42 and 43, it is concluded that in a bipolar three-dimensional electrode working with the cathodic side under limiting current conditions the optimal bed thickness is lower than those of a monopolar electrode under the same operative conditions. This behaviour is explained by stating that the leakage current increases the potential distribution inside the electrode.

## 3 Experimental

The experiments were performed in a flow-by electrochemical reactor, schematically shown in Fig. 3a, made of

three compartments. The external compartments contain the terminal electrodes and the one in the middle, the bipolar electrode. The terminal electrodes were made of 10 segments of nickel positioned near the separator and inclined 30° from the vertical to deviate the gases to the backside of the electrodes. This inclination angle is in the optimal range recommended by Kreysa and Külps [34] for gas evolving electrodes. A calibrated resistor made from constantan wire, 100 mm long, 1.5 mm diameter and approximately 0.02 Ω resistance, was intercalated between the backside of each segment and the current feeder of the terminal electrode. By measuring the ohmic drop in the corresponding resistor, it was possible to determine the axial current distribution at each terminal electrode. The projected area of each segment on the separator was $1 \times 5$ cm$^2$ and the backside of each segment was covered with epoxy resin to make it non-conductive. The data acquisition was performed with an analogue multiplexer commanded by a computer. The influence of these resistors on the cell voltage is negligible due to the small value of its resistance.

The bipolar electrode was a stack of nets fabricated from rectangular plates, 50 mm × 100 mm, which were welded at several points in the perimeter to obtain mechanical stability of the structure and to ensure isopotentiality of the metal phase. The cathodic part of the bipolar electrode was made from a 304 stainless steel woven-wire mesh, 50 mesh size (0.177 mm wire diameter and 0.331 mm distance between wires), whereas a similar copper mesh was used for the anodic region. The average value of the geometric specific surface area was approximately 6,420 m$^{-1}$ with a void fraction of 0.70. The thickness of the bipolar electrode was 17 mm. The bipolar electrode was separated from the terminal electrodes by cationic exchange membranes.

Owing to the special construction of this reactor, the primary current distribution is uniform. Likewise, to achieve more uniform mass-transfer conditions along the reactor, flow distributor plates with 149 holes, 1.5 mm in diameter, were arranged in the inlet and outlet of the electrolyte in each compartment. The reactor was made part of two flow circuit systems, as shown in Fig. 3b, consisting of pumps, flow meter and connections to maintain the temperature at the preset value (30 °C). In all experiments, the volumetric flow rate in the bipolar electrode was $6.06 \times 10^{-6}$ m$^3$ s$^{-1}$.

The experiments were carried out galvanostatically; two saturated calomel electrodes were used as reference electrodes, each being connected to Haber–Luggin capillaries positioned at both sides of the bipolar electrode.

The electrolyte solution in the bipolar electrode was 1 M $Na_2SO_4$ and $H_2SO_4$, to obtain pH 2, with a copper concentration of approximately 600 ppm. During the experiment, samples of solution were taken at intervals from the reactor outlet to determine the copper concentration by

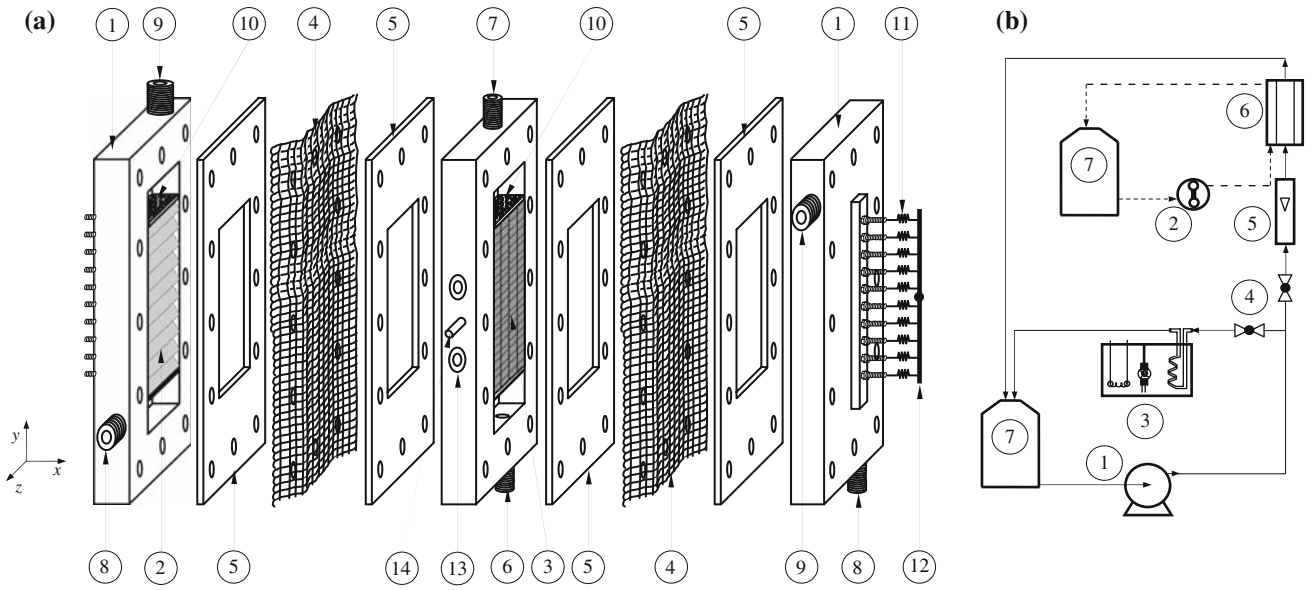


**Fig. 3** **a** Exploded view of the electrochemical reactor with a bipolar three-dimensional electrode. 1—terminal plates, 2—segmented inclined terminal electrodes, 3—bipolar three-dimensional electrode, 4—cationic exchange membranes, 5—gaskets, 6—electrolyte inlet, 7—electrolyte outlet, 8—NaOH solution inlet, 9—NaOH solution outlet, 10—flow distributor plates, 11—calibrated resistors, 12—electrical connexion to the terminal electrodes, 13—ports for the Haber–Luggin capillaries, 14—electrical connexion to measure the potential of the bipolar electrode. **b** Scheme of the electrolyte circulation systems. *Full line*: solution in the bipolar electrode; *dashed line*: NaOH solution for the terminal electrodes. 1—centrifugal pump, 2—peristaltic pump, 3—thermostat, 4—valves, 5—flow meter, 6—electrochemical reactor, 7—reservoirs

complexometry. A solution of 1 M NaOH was used in the terminal compartments, hydrogen and oxygen evolution were the cathodic and anodic reactions at the terminal electrodes.

After the experiments, some epoxy resin was poured into the three-dimensional bipolar electrode and cured. Cross-sections of the electrode were polished and examined with a metallurgical microscope to determine the thickness distribution of the deposit and the diminution of the wire diameter in the anodic region along the electrode thickness.

According to the Faraday law, the change in radius of a wire in the three-dimensional electrode is related to the local current density by the following equation

$$\Delta r(x) = -\frac{M j(x) t}{v_e \mathrm{F} \delta}. \tag{44}$$

At low overpotentials Eq. 12 is simplified to

$$j(x) = \frac{\frac{v_e \mathrm{F}}{\mathrm{R}T}\eta(x)}{\left(\frac{1}{j_0} - \frac{1}{j_L}\right) + \frac{\beta \mathrm{F}}{j_L \mathrm{R}T}\eta(x)}. \tag{45}$$

Taking the first derivative of Eq. 45 evaluated at $x = L_c$ is

$$\left.\frac{\mathrm{d}\eta(x)}{\mathrm{d}x}\right|_{x=L_c} = \frac{\mathrm{R}T}{v_e \mathrm{F}}\left(\frac{1}{j_0} - \frac{1}{j_L}\right)\left.\frac{\mathrm{d}j(x)}{\mathrm{d}x}\right|_{x=L_c}. \tag{46}$$

Combining Eqs. 11, 44 and 46 and rearranging, the leakage current was calculated by

$$I^* = -\frac{S\mathrm{R}T\delta}{\rho_s M t}\left(\frac{1}{j_0} - \frac{1}{j_L}\right)\left.\frac{\mathrm{d}\Delta r(x)}{\mathrm{d}x}\right|_{x=L_c}. \tag{47}$$

The slope of the thickness variation at $L_c$ was determined by a linear fitting of the experimental results.

## 4 Results and discussion

Figure 4 shows the current at the terminal electrodes as a function of the axial position $y$. The vertical bar represents the standard error of the mean. It can be observed that, in spite of the symmetrical arrangement of the reactor, the axial current distribution of the terminal anode is more uniform than that of the terminal cathode; for which a sheer change in the current is mainly detected in the inlet region of the reactor. This behaviour can be attributed to the anodic reaction at the bipolar electrode because the polarization resistance for the copper dissolution decreases suddenly when the current increases. Thus, the copper dissolution is favoured in the inlet region where the concentration can be smaller.

Figure 5 reports some micrographs of cross-sections of wires, magnification ×100, in the three-dimensional bipolar electrode to show the dependence of the morphology

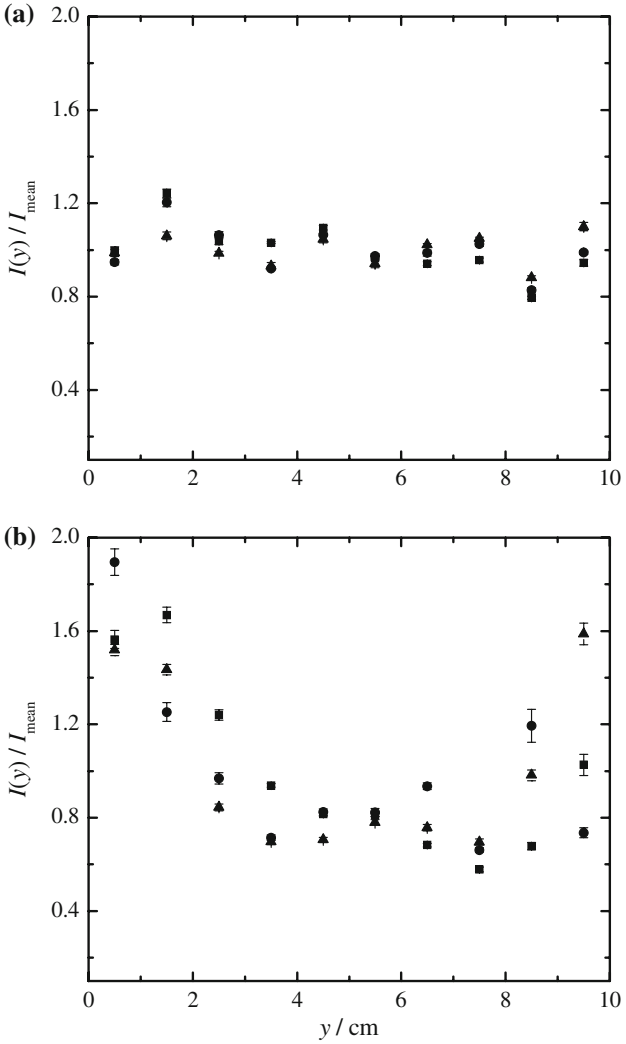


**Fig. 4** Current as a function of the axial position. **a** Terminal anode; **b** Terminal cathode. *Filled square*: $I = 2.0$ A; *Filled circle*: $I = 2.5$ A; *Filled triangle*: $I = 3.0$ A. *Vertical bars*: standard error of the mean

with the position, $x$ and $z$ coordinates. The deposits obtained near the terminal anode show dendritic characteristics. Those electrodeposited in the central part are nodular, and a more compact nature is detected in the deposited copper in the region far from the terminal anode, where lower values of overpotential are achieved. As expected, a more dendritic nature was observed when the current is increased. Furthermore, the deposits generally show a similar thickness in all the perimeter of a wire. However, some abnormal situations were observed in the intersection between two wires; where, due to the shielding effect, the thickness of the deposit is lower in the contact region of the wires. In the anodic part of the bipolar electrode, a high non-uniformity was observed for the copper dissolution.

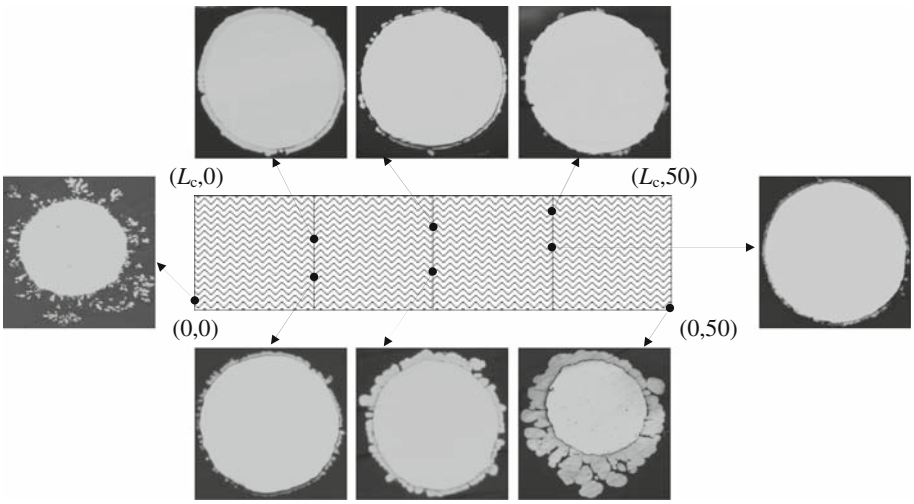


**Fig. 5** Morphology of the deposits as a function of the position in the cross-sectional area for the cathodic side of the three-dimensional bipolar electrode. $I = 2$ A, $t = 360$ min, $y = 50$ mm. Dimensions of the $x$ and $z$ coordinates in mm. Magnification $\times 100$

Figure 6 shows the change of the wire radius along the electrode thickness, $x$ coordinate, at $y = 5$ cm for a typical experiment. Each point is the mean value, which was determined with an image analysis and processing software, of the radius change at five different positions along the electrode width, i.e. at both edges, in the centre and in the middle regions between them. The vertical bar represents the standard error of the mean. Due to the anisotropy of the three-dimensional electrode, the $\Delta r$ distribution depends on the $z$ values. However, the same tendency was observed in all cases. The full line represents the theoretical behaviour. A close agreement between experimental and theoretical results is obtained in the middle of the cathodic region of the bipolar electrode. The measurement of the deposit thickness near the terminal anode is quite insecure due to the dendritic nature of the deposits and the deposit thickness is small in the region of low cathodic overpotentials. A high scattering of the experimental results is observed in the anodic part of the bipolar electrode due to the non-uniform dissolution of copper. The inset in Fig. 6 shows the cathodic region at low overpotentials, its slope was used in Eq. 47 to estimate the leakage current in the bipolar electrode. In some experiments, a high discrepancy was observed between the experimental and theoretical overpotentials at both sides of the bipolar electrode. This can be explained taken into account that in the first place the experimental values were measured in only one point in the periphery of the electrode, and second that the bipolar electrode shows an important overpotential variation with the position, mainly in the anodic region. Table 2 summarizes the results of the experiments performed at different total currents, where a close agreement can be observed between the calculated and measured values of the thickness of the cathodic part at the bipolar electrode, $L_c$. Likewise, the theoretical by-passed fraction of the total current well agrees with the estimated values from the experimental results.

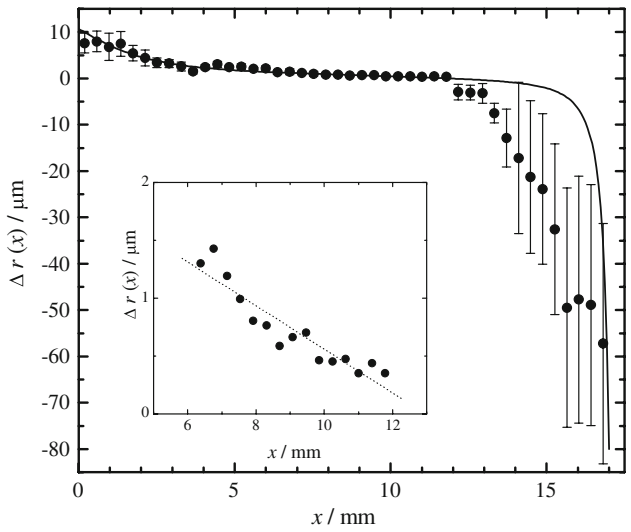


**Fig. 6** Mean value of the change of wire radius as a function of the $x$ coordinate at $y = 50$ mm, $I = 2.5$ A. *Vertical bars*: standard error of the mean. *Full line*: theoretical prediction. Inset: enlargement of the cathodic region at low overpotentials. *Dotted line*: linear correlation

Figure 7 reports the theoretical values of $\psi$ as a function of the total current. The diminution of $\psi$ can be explained considering that in a bipolar reactor there are two paths for the flow of current: (i) the faradaic path where the current flows through the bipolar electrodes and (ii) the by-passed path where the bipolar electrodes are excluded. The former

**Table 2** Summary of experimental results

| $I$ (A) | $t$ (min) | $C_{mean}$ (ppm) | $L_c\|_{exp}$ (mm) | $L_c\|_{th}$ (mm) | $\psi\|_{exp}$ (%) | $\psi\|_{th}$ (%) |
|---|---|---|---|---|---|---|
| 2 | 360 | 617 | 12 | 11.56 | 5.89 | 5.75 |
| 2.5 | 180 | 580 | 12 | 11.79 | 3.81 | 5.39 |
| 3 | 180 | 588 | 12 | 12.06 | 8.29 | 5.53 |

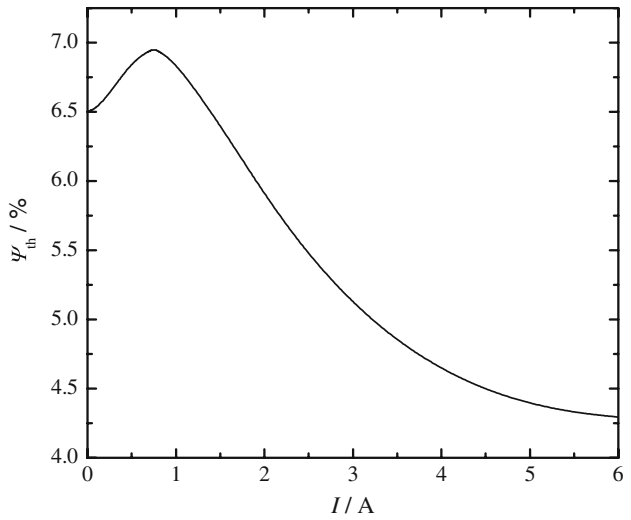


**Fig. 7** Theoretical by-passed current fraction as a function of the total current. Kinetics: diffusion and charge-transfer control. Parameters according to Table 1. $A_s = 6{,}420\ m^{-1}$, $\varepsilon = 0.7$, $C = 600$ ppm

is characterized by the polarization resistance and the latter by the electrolyte resistance inside the electrode. When the faradaic current increases the polarization resistance also increases and the by-passed path is favoured. Thus, the leakage current is enlarged. However, the increase in the faradaic current is higher than that in the leakage current and $\psi$ decreases when the current increases. The contrary behaviour is observed at low currents.

## 5 Conclusions

(i) A suitable agreement, within the accuracy expected for experiments involving metal deposition, was achieved between the experimental results of thickness distribution and theoretical calculations. These were obtained from the solution of a model for bipolar three-dimensional electrode taken into account the leakage current.

(ii) The electrochemical reactor shows axial current distribution as a consequence of the polarization resistance of the anodic reaction at the bipolar electrode.

(iii) The electrodeposited metal thickness varies with the position along the electrode width due to the non-uniformity of the solution flow inside the electrode.

(iv) Different morphological electrodeposits are obtained along the cathodic bed thickness due to the overpotential distribution in this coordinate.

**Acknowledgements** This study was supported by the Agencia Nacional de Promoción Científica y Tecnológica (ANPCyT), Consejo Nacional de Investigaciones Científicas y Técnicas (CONICET) and Universidad Nacional del Litoral (UNL) of Argentina.

## References

1. Pletcher D, Walsh FC (1993) Industrial electrochemistry, Chap. 2. Chapman and Hall, London, pp 136–141
2. Goodridge F, Wright AR (1983) In: Yeager E, Bockris JO'M, Conway BE, Sarangapani S (eds) Comprehensive treatise of electrochemistry, vol 6, Chap. 6. Plenum Press, New York, pp 429–430
3. Alkire R (1973) J Electrochem Soc 120:900
4. Fleischmann M, Ibrisagić Z (1980) J Appl Electrochem 10:151
5. Goodridge F, King CJH, Wright AR (1977) Electrochim Acta 22:347
6. Goodridge F, King CJH, Wright AR (1977) Electrochim Acta 22:1087
7. Goodridge F (1977) Electrochim Acta 22:929
8. Kusakabe K, Morooka S, Kato Y (1982) J Chem Eng Jpn 15:45
9. Kusakabe K, Kimura T, Morooka S, Kato Y (1984) J Chem Eng Jpn 17:293
10. Miyazaki Y, Katagiri A, Yoshizawa S (1987) J Appl Electrochem 17:113
11. Sasaki T, Ishikawa T (1984) Denki Kagaku 52:318
12. Cheng CY, Kelsall GH, Pilone D (2005) J Appl Electrochem 35:1191
13. Sasaki T, Ishikawa T (1986) Electrochim Acta 31:745
14. Nadebaum PR, Fahidy TZ (1975) J Electrochem Soc 122:1035
15. Nadebaum PR, Fahidy TZ (1975) J Appl Electrochem 5:249
16. Fleishmann M, Ghoroghchian J, Jansson REW (1981) J Appl Electrochem 11:55
17. Bakir Ogutveren U, Plimley RE, Nieva I (1992) J Appl Electrochem 22:351
18. Güvenç A, Tarik Pekel A, Mete Koçkar Ö (2004) Chem Eng J 99:257
19. Boussoulengas AV, Ehadaie S, Jansson REW (1979) Chem Ind October:6
20. Ellis KG, Jansson REW (1981) J Appl Electrochem 11:531
21. Franke L, Zimmer A, Seibig K (1992) Chem Ing Tech 7:652
22. Kim HJ, Kusakabe K, Hokazono S, Morooka S, Kato Y (1987) J Appl Electrochem 17:1213
23. Gupta N, Oloman CW (2006) J Appl Electrochem 36:255
24. Ehadaie S, Fleischmann M, Jansson REW (1982) J Appl Electrochem 12:59
25. Cox DA, El-Ghaoui EA, Ellis KG, Jansson REW, Meissner D (1982) J Chem Tech Biotechnol 32:462
26. Kusakabe K, Kimura T, Morooka S, Kato Y (1987) J Appl Electrochem 17:724
27. Grau J, Bisang JM (2009) J Chem Technol Biotechnol 84:1084
28. Cœuret F, Storck A (1984) Elements de Genie Electrochimique, Chap. 3b. TEC&DOC, Paris, p 159
29. Storck A, Robertson PM, Ibl N (1979) Electrochim Acta 24:373
30. Kusik CL, Meissner HP (1978) AIChE Symp Ser 74:14
31. Burnett JC, Danly DE (1979) AIChE Symp Ser 75:8
32. Wagner C (1951) J Electrochem Soc 98:116
33. Kreysa G (1983) Dechema Monographs 94:123
34. Kreysa G, Külps H-J (1981) J Electrochem Soc 128:979